Characteristics of betatron radiation from direct-laser-accelerated electrons

T. W. Huang,[1,2] A. P. L. Robinson,[2,*] C. T. Zhou,[1,3,4,†] B. Qiao,[1,‡] B. Liu,[1,3] S. C. Ruan,[4] X. T. He,[1,3] and P. A. Norreys[2,5]

[1]*HEDPS, Center for Applied Physics and Technology and School of Physics, Peking University, Beijing 100871, People's Republic of China*

[2]*Central Laser Facility, STFC Rutherford-Appleton Laboratory, Didcot, OX11 0QX, United Kingdom*

[3]*Institute of Applied Physics and Computational Mathematics, Beijing 100094, People's Republic of China*

[4]*College of Electronic Science and Technology, Shenzhen University, Shenzhen 518060, People's Republic of China*

[5]*Clarendon Laboratory, Department of Physics, University of Oxford, Parks Road, Oxford, OX1 3PU, United Kingdom*

(Received 17 February 2016; published 8 June 2016)

Betatron radiation from direct-laser-accelerated electrons is characterized analytically and numerically. It is shown here that the electron dynamics is strongly dependent on a self-similar parameter $S(\equiv \frac{n_e}{n_c a_0})$. Both the electron transverse momentum and energy are proportional to the normalized amplitude of laser field (a_0) for a fixed value of S. As a result, the total number of radiated photons scales as $a_0^2/\sqrt{S}$ and the energy conversion efficiency of photons from the accelerated electrons scales as a_0^3/S. The particle-in-cell simulations agree well with the analytical scalings. It is suggested that a tunable high-energy and high-flux radiation source can be achieved by exploiting this regime.

DOI: 10.1103/PhysRevE.93.063203

I. INTRODUCTION

The generation of compact radiation sources has attracted great attention because of its significance in many research communities and industrial applications [1,2]. With the rapid development of high power lasers, laser-based radiation sources have become an important complement to the conventional synchrotron light sources [3]. Laser-based radiation sources could, potentially, be much smaller and cost effective compared with conventional light sources. For a high power laser beam propagating into the underdense plasma, its ponderomotive force expels the electrons from the high-intensity regions to form an ion channel or cavity, in which the electrons experience transverse betatron oscillations under the self-generated magnetic and electrostatic fields of the plasma channel. As a result, broadband and synchrotronlike radiation can be generated from the oscillating electrons [3–24]. The synchrotron radiation is strongly dependent on the betatron strength parameter $a_\beta = \gamma r_\beta \omega_\beta / c$, which is proportional to the Lorentz factor of the electron γ and the transverse oscillation amplitude of betatron motion r_β, as well as the betatron frequency ω_β [3–5]. It is noted that both the radiated photon energy and number are proportional to the betatron strength parameter. The production of a high-flux and high-energy radiation source requires the enhancement of both the energy and betatron amplitude of the electrons in the plasma channel.

One promising way to enhance both the energy and betatron amplitude of the electron is the resonance between the betatron oscillation of the electron in a plasma channel and the laser field. This can be easily achieved in the direct laser acceleration (DLA) regime [25–31] and high brightness synchrotron x rays and γ rays can be produced [15–17]. In the laser wakefield acceleration (LWFA) regime, this can also be achieved by interacting the injected electrons with the tail of the driving laser pulse when the laser pulse duration is comparable to the plasma period [18–24]. In this situation, the interaction of the laser pulse with the accelerated electrons can enhance the transverse amplitude of the electron motion along the polarization direction, thus the number and energy of the emitted photons can be much increased and γ-ray photons have been observed in the experiment [24]. However, the number of high-energy electrons generated in the LWFA regime is still relatively low, which would impose restrictions on the number of emitted photons and thus the brightness of the radiation source. In the DLA regime of ultraintense laser pulses interacting with the near-critical dense plasmas, a high-energy and high-current electron beam with a large betatron amplitude can be easily produced [30,31]. This would be promising for the production of a high-flux and high-energy radiation source. However, to date the fundamental scalings of the electron dynamics and the emitted photons have not been studied for the case of direct-laser-accelerated electrons. Understanding the underlying dependence of the radiation properties on some controllable parameters such as the plasma density, the laser intensity, and the interaction length is necessary for the development and optimization of the x-ray or γ-ray sources.

In this work, the underlying scalings of the direct-laser-accelerated electrons and the radiated photons are investigated in the DLA regime of an ultraintense laser pulse interacting with a uniform near-critical density plasma. The dependence of the radiation properties on the plasma density and laser intensity is given analytically. It is shown that the electron dynamics and the emitted photons are strongly dependent on a self-similar parameter $S \equiv \frac{n_e}{n_c a_0}$. This controls the energy gain and the transverse betatron amplitude of the electrons, as to the radiated photon number and photon energy. In addition, the model indicates that the total number of photons is proportional to a_0^2 and the energy conversion efficiency of the photons from the accelerated electrons is proportional to a_0^3 for a fixed value of S. These nonlinear scalings on the laser amplitude suggest that a high-flux and high-energy radiation source can be easily achieved by increasing the laser amplitude in the DLA regime.

The paper is organized as follows. In Sec. II, the electron acceleration process in the DLA regime is explored analytically. The resulting betatron radiation emission and its

*alex.robinson@stfc.ac.uk

†zcangtao@iapcm.ac.cn

‡bqiao@pku.edu.cn

 ©2016 American Physical Society

optimization are described in Sec. III. The parameters and results of supporting two- and three-dimensional particle-in-cell simulations are described in Sec. IV. In Sec. V, the limitations imposed by the experimental parameters on the source brightness are discussed, including dephasing and depletion effects. The work is then summarized in Sec. VI.

II. ELECTRON ACCELERATION

In the interaction of an ultraintense short laser pulse with undercritical plasma ($\frac{n_e}{n_c a_0} \ll 1$), electrons are accelerated to a highly relativistic energy with relatively good efficiency. Here n_e is the plasma density, n_c is the critical plasma density, and a_0 is the normalized amplitude of the laser beam. The electron acceleration mechanisms strongly depend on the laser and plasma parameters [25–42]. For a short laser pulse with the duration (τ) shorter than or comparable to $1/\omega_p$, i.e., $\tau \leqslant 1/\omega_p$, where ω_p is the plasma frequency, the laser wakefield acceleration would play the dominant role [32–37]. When the pulse duration is longer than $1/\omega_p$ and $a_0 \cong 1$, the laser envelope is self-modulated by the plasma wave and the electrons are accelerated by a self-modulated laser wakefield [38–40]. However, for the laser pulse with $\tau > 1/\omega_p$, with the increase of the laser intensity the plasma wave breaking destroys the periodic structure and the laser ponderomotive force expels the electrons from the central regions to form a plasma channel. In this case the electron can be directly accelerated by the laser pulse when its oscillation frequency in the fields of the plasma channel is close to the Doppler-shifted laser frequency [25–31]. In this regime of direct-laser acceleration, electrons gain their energy mainly from the transverse laser field, in contrast to the longitudinal charge separation field in the laser wakefield regime. In addition, the transverse oscillation amplitude can also be enhanced and a large betatron strength parameter can be realized in this regime [15–24].

In order to investigate the characteristics of the direct-laser-accelerated electrons, the dynamics of a single electron interacting with the laser field and the self-generated fields of the plasma channel is considered. One can first assume a linearly polarized plane wave with the transverse electromagnetic fields as $E_{Ly} = E_0 \cos(\phi)$ and $B_{Lz} = E_{Ly}/v_{\rm ph}$, where E_0 is the amplitude of the laser field, $\phi = kx - \omega_0 t$ is the laser phase, x is the laser propagation direction, ω_0 is the laser frequency, k is the wave number, and $v_{\rm ph} = \omega_0/k$ is the phase velocity. The transverse self-generated fields in the plasma channel are assumed to be E_{Sy}, E_{Sz}, B_{Sy}, and B_{Sz}. For the electron interacted with a linearly polarized laser pulse, the electron is preferentially accelerated along the laser polarization direction [42]. In this case, the electron dynamics can be described by the momentum equation along the laser polarization direction coupled with the energy equation:

$$\frac{dp_y}{dt} = -e\eta E_0 \cos(\phi) - eE_{Sy} + ev_x B_{Sz}, \tag{1}$$

$$m_e c^2 \frac{d\gamma}{dt} = -ev_y E_0 \cos(\phi) - ev_z E_{Sz} - ev_y E_{Sy}, \tag{2}$$

where $\eta = 1 - v_x/v_{\rm ph}$, m_e is the rest electron mass, c is the light speed in vacuum, and $\gamma = \sqrt{1 + (\frac{p_x}{m_e c})^2 + (\frac{p_y}{m_e c})^2 + (\frac{p_z}{m_e c})^2}$ is the Lorentz factor of the electron. The longitudinal momentum of the electron is obtained from the integral of motion for the electron, which can be expressed as $I \equiv \gamma m_e c^2 - v_{\rm ph} p_x + e(\kappa_E + v_{\rm ph}\kappa_B) r^2/2$, where $\kappa_E = \partial E_{Sy}/\partial y = \partial E_{Sz}/\partial z$, $\kappa_B = \partial B_{Sy}/\partial z = -\partial B_{Sz}/\partial y$, $r^2 = y^2 + z^2$, and I is a constant decided by the initial condition of the electron. For a uniform plasma channel, one can easily show that $e\kappa_E = (1-f) m_e \omega_p^2/2$ and $e\kappa_B = f m_e \omega_p^2 v_x/2c^2$, where $0 \leqslant f \leqslant 1$ refers to the percentage of electrons in the plasma channel [43,44]. It is noted that the model described here is similar to the previous ones [28,30,42]. These models describe the similar electron acceleration process, i.e., the so-called direct-laser acceleration or betatron resonance acceleration. Several different regimes in DLA have been proposed and studied in previous works [28,30,42]. However, no scaling studies on the quality of both the electron and radiation source have been presented. Here we are concentrated on the scaling studies of electron dynamics in the plasma channel, which is crucial to exploit the scaling properties of betatron radiation in the DLA regime. This is an essential step to develop and optimize the radiation source in this regime.

For resonant electrons, whose velocity would be close to c, one assumes that $dv_x/dt \approx 0$ and $d\eta/dt \approx 0$ as v_x is a slow variable compared with the fast variables of y and p_y. In this case, the phase witnessed by the relativistic electron is written as $\phi = kx - \omega_0 t \approx \omega_L t$, where $\omega_L = (1 - v_x/v_{\rm ph})\omega_0 = \eta\omega_0$ is the Doppler-shifted laser frequency. Under these assumptions, Eqs. (1) and (2) are simplified to [45]

$$\frac{d^2 p_y}{dt^2} + \omega_\beta^2 p_y = m_e c a_0 \omega_L^2 \sin(\omega_L t), \tag{3}$$

$$\gamma \frac{d\gamma}{dt} = -\omega_0 p_y a_0 \cos(\omega_L t)/m_e c, \tag{4}$$

where $\omega_\beta = \sqrt{e(\kappa_E + v_x\kappa_B)/\gamma m_e}$ is the betatron frequency and $a_0 = eE_0/m_e\omega_0 c$ is the normalized amplitude of the laser field. For the resonant electrons with $v_x \approx c$, $e(\kappa_E + v_x\kappa_B) = (1-f) m_e\omega_p^2/2 + f m_e \omega_p^2 v_x^2/2c^2 \approx m_e\omega_p^2/2$ and $\omega_\beta \approx \omega_p/\sqrt{2\gamma}$. It is noted here that the value of f does not affect the electron dynamics. The above equations clearly reveal the scheme of electron acceleration. In this case, when the betatron frequency varies roughly twice the laser frequency, the classical betatron resonance is extended to the nonlinear parametric resonance regime [42,45] in which the electron transverse momentum grows nonlinearly with time and grows faster than the classical linear resonance [45].

One can further employ the dimensionless variables $Q = \frac{p_y}{a_0 m_e c}$ and $G = \frac{\gamma}{a_0}$. Equations (3) and (4) are rewritten as $\frac{d^2 Q}{dt^2} + \omega_\beta^2 Q = \omega_L^2 \sin(\omega_L t)$ and $G\frac{dG}{dt} = -\omega_0 Q \cos(\omega_L t)$. This shows that the electron dynamics are determined by a single parameter of ω_L or η. For an ultraintense laser pulse propagating in the underdense plasma, $n_e/a_0 n_c \ll 1$, then one has $v_{\rm ph} = c/\sqrt{1 - \frac{\omega_p^2}{\gamma_L \omega_0^2}} \approx c(1 + \frac{n}{2\gamma_L})$ and $\eta = 1 - v_x/v_{\rm ph} \approx n/2\gamma_L \approx n/\sqrt{2}a_0$, where $\gamma_L = \sqrt{1 + a_0^2/2} \approx a_0/\sqrt{2}$ is the averaged Lorentz factor and $n = \omega_p^2/\omega_0^2 = n_e/n_c$ is the normalized plasma density. Clearly, the electron dynamics is strongly

dependent on the self-similar parameter of n/a_0 [45,46]. Once the value of n/a_0 is fixed, the electron dynamics is determined and the normalized parameters of $\frac{p_y}{a_0 m_e c}$ and $\frac{\gamma}{a_0}$ are also fixed.

For direct-laser-accelerated electrons, their maximum energy is determined by the resonance condition with $\omega_\beta \approx \omega_L = \eta\omega_0 \approx \omega_0 n/\sqrt{2}a_0$. From this one can obtain the energy of the resonant electrons as $\gamma_\beta \approx a_0^2/n$. For the betatron oscillation, the electron transverse momentum is expressed as $p_\beta/m_e c \approx \gamma\omega_\beta r_\beta/c$. Here r_β is the excursion of the electron, which reaches a maximum value comparable to the radius of the laser beam as the resonant electrons only locate in the laser region. For the self-matched propagation of relativistic laser pulse in underdense plasma, the radius of the laser beam is about twice the relativistically corrected plasma skin depth $2\sqrt{\gamma_L}c/\omega_p$ [47–49]. Then the maximum electron transverse momentum can be written as $p_\beta/m_e c \approx 2^{1/4}a_0\sqrt{\frac{a_0}{n}}$. This shows that the normalized parameter $\frac{\gamma_\beta}{a_0}$ scales as $\frac{a_0}{n}$ and $\frac{p_\beta}{a_0 m_e c}$ scales as $\sqrt{\frac{a_0}{n}}$.

In addition, an electron only gains energy from the laser pulse when it stays in phase with the laser electric field. The acceleration length for the DLA electrons is determined by the dephasing length when the laser pulse is long enough so that the depletion length of the laser pulse is larger than the dephasing length. In this case, the electrons resonantly interact with the laser pulse adequately and gain energy continuously until the dephasing occurs. The dephasing rate between the electrons and the laser field can be expressed as $\frac{d\phi_\beta}{dt} = \omega_\beta - \omega_0(1 - \frac{v_x}{v_{\rm ph}})$, where ϕ_β refers to the relative phase between the electron oscillation and the laser field. It is noted that when the betatron frequency ω_β gets close to the Doppler-shifted laser frequency, the dephasing phase changes slowly so that the electrons stay in phase with the laser pulse for a long time and gain significant energy. However, the damping effect caused by the increase of the Lorentz factor will shift the resonance condition to be $\omega_\beta = (1-\delta)\omega_L$, where δ refers to the frequency deviation and is proportional to the damping rate $\frac{d\gamma/dt}{\gamma}$ [45]. In this case, the acceleration time of the electron is expressed as $T_{dp} \approx \frac{\pi}{|d\phi_\beta/dt|} \approx \frac{T_L}{\sqrt{2}|\delta|}\frac{a_0}{n}$, which is inversely proportional to the value of $\frac{n}{a_0}$. Here T_L refers to the period of the laser pulse. This model now indicates that the self-similar parameter n/a_0 controls both the energy gain and the transverse oscillation amplitude of the electron, as well as the acceleration length.

III. BETATRON RADIATION

Betatron radiation can be generated when the relativistic electrons experience transverse betatron oscillations in the plasma channel. The theoretical properties of betatron radiation are well known [3–7]. The betatron radiation is characterized by a betatron strength parameter with $a_\beta = \gamma r_\beta \omega_\beta/c$. Both the emitted photon energy and number are proportional to a_β. In the wiggler limit of $a_\beta \gg 1$, the radiation spectrum becomes quasicontinuous and consists of a series of harmonics with a critical energy of $E_c = 3\hbar a_\beta \gamma^2 \omega_\beta$ and the number of photons emitted by the electron scales as $N_\beta \sim N a_\beta$, where $\hbar$ is the Planck constant and N denotes the number of betatron oscillations [3–7]. The generated radiation is confined into a narrow cone with opening angle about $\theta \approx a_\beta/\gamma$.

The radiation properties are strongly dependent on the electron dynamics, which in turn depends on the choice of different laser and plasma parameters. It is noted here that the betatron strength parameter a_β also represents the transverse momentum of the electron $p_\beta/m_e c$. For direct-laser-accelerated electrons, the value of a_β is $a_\beta \approx p_\beta/m_e c \approx 2^{1/4}a_0\sqrt{\frac{a_0}{n}}$. This shows that an extremely large betatron strength parameter is achieved for a small value of n/a_0 with a large laser amplitude a_0. One can further express the critical energy of the photon as $E_c \approx 2.5\hbar\omega_0 a_0^3(\frac{a_0}{n})^{3/2}$ and the number of photons emitted by the resonant electrons scales as $N_\beta \sim \omega_\beta T_{dp} a_\beta \sim a_0\sqrt{\frac{a_0}{n}}\pi$. The divergence angle of the radiation is about $\theta \approx 2^{1/4}\sqrt{n/a_0}$. The total radiation energy is written as $W_{\rm ph} \approx N_e N_\beta E_c$ and the total number of photons is $N_{\rm ph} \approx N_e N_\beta$, where N_e is the total number of resonant electrons. For a laser beam with a matched radius of $R \approx 2\sqrt{\gamma_L}c/\omega_p$, a stable plasma channel is then formed. One estimates the number of resonant electrons confined in the plasma channel to be $N_e \approx n_e \pi R^2 c\tau \sim a_0 n_c \lambda_L^2 c\tau$, where τ is the duration of the laser pulse and λ_L is the laser wavelength. Then the total energy of accelerated electrons can be estimated as $W_{\rm ele} \approx \gamma m_e c^2 N_e$. Based on these assumptions, the total number of photons scales as $N_{\rm ph} \propto a_0^2\sqrt{\frac{a_0}{n}}$ and the conversion efficiency of direct-laser-accelerated electrons into high-energy photons scales as $W_{\rm ph}/W_{\rm ele} \approx E_c N_\beta/\gamma \propto a_0^3\frac{a_0}{n}$. Thereby, for direct-laser-accelerated electrons, the dependence of the corresponding radiation on the laser intensity and plasma density can be described as

$$E_c \propto a_0^3\left(\frac{a_0}{n}\right)^{3/2}, \quad N_{\rm ph} \propto a_0^2\left(\frac{a_0}{n}\right)^{1/2}, \quad \theta \propto \left(\frac{n}{a_0}\right)^{1/2}, \tag{5}$$

$$\frac{W_{\rm ph}}{W_{\rm ele}} \propto a_0^3\left(\frac{a_0}{n}\right). \tag{6}$$

It is noted that these scalings are quite different from that in the laser wakefield acceleration regime. For laser-wakefield-accelerated electrons, if the possible interaction between the electron beam and the laser pulse is not considered, the generated radiation displays scalings as [3]

$$E_c \propto a_0\left(\frac{a_0}{n}\right)^{3/2}, \quad N_{\rm ph} \propto a_0\left(\frac{a_0}{n}\right)^{3/2}, \quad \theta \propto n^{1/2}, \tag{7}$$

$$\frac{W_{\rm ph}}{W_{\rm ele}} \propto a_0\left(\frac{a_0}{n}\right)^{3/2}. \tag{8}$$

This shows that for a fixed value of n/a_0, radiation from the direct-laser-accelerated electrons reveals nonlinear scalings on the laser amplitude as $E_c \propto a_0^3$, $N_{\rm ph} \propto a_0^2$, and $W_{\rm ph}/W_{\rm ele} \propto a_0^3$, in contrast to the linear scalings for the laser-wakefield-accelerated electrons as $E_c \propto a_0$, $N_{\rm ph} \propto a_0$, and $W_{\rm ph}/W_{\rm ele} \propto a_0$. This indicates that it is much easier to produce a high-energy and high-flux radiation source by employing an ultraintense laser pulse interacting with the underdense plasma in the DLA regime. Exploiting these scalings is significant

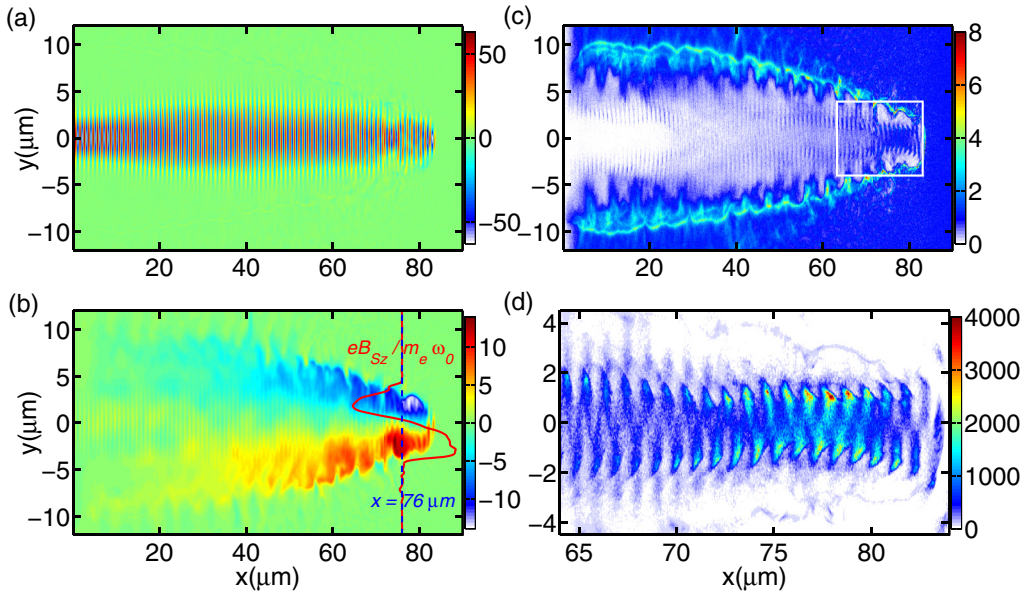

FIG. 1. 2D particle-in-cell simulation results for $a_0 = 60$ and $n_e = 1.8n_c$ at $T = 100T_L$. (a) The distribution of the normalized transverse laser field ($eE_y/m_e\omega_0 c$). (b) The corresponding azimuthal static magnetic field ($eB_{Sz}/m_e\omega_0$) generated by the fast electrons confined in the plasma channel, where the red line shows the transverse profile of the static magnetic field at $x = 76$ μm. (c) The distribution of normalized electron density (n_e/n_0), where n_0 refers to the initial plasma density. (d) The distribution of the normalized electron energy density ($n_e E_e/n_c m_e c^2$) in the white rectangle region shown in (c), where E_e is the averaged electron energy on each grid.

for the development and optimization of a high-energy and brightness radiation source.

IV. PARTICLE-IN-CELL SIMULATIONS

In order to test the analytical scalings predicted in the above section, two-dimensional (2D) and three-dimensional (3D) particle-in-cell (PIC) simulations were carried out using the code EPOCH [50]. In the simulations, a p-polarized Gaussian laser beam with a self-matched radius of $2\sqrt{\gamma_L}c/\omega_p$ was irradiated into a uniform near-critical density plasma. The central laser wavelength is $\lambda = 1$ μm and the duration of the laser pulse is initially fixed as $100T_L$. The depletion length of such a long laser pulse is ensured to be larger than the dephasing length between the electron oscillation and the laser field. The grid size is set as $1/40$ μm along the propagation direction and $1/20$ μm in transverse plane. 25 particles of each species (electron and ion) are put in each cell. The initial electron temperature is assumed to be 1 keV. Different laser intensities and plasma densities are considered to characterize the scaling properties of the electron dynamics and the generated radiation. In the simulations, the radiation recoil effect is self-consistently considered.

Figures 1–3 show the simulation results for a laser pulse with the peak intensity of 4.9×10^{21} W/cm^2 propagating through a near-critical density plasma with $n_e = 1.8n_c$. The initial radius of the laser beam is set as 2.2 μm, which is about twice the relativistically corrected plasma skin depth; this ensures that the laser beam can match well with the plasma and stably propagate into the plasma [47]; as shown in Fig. 1(a), no obvious self-focusing and filamentation instability are observed. The normalized amplitude of the laser pulse is close to its initial value with $a_0 = 60$. Figure 1(c) shows that a stable plasma channel is formed by the laser ponderomotive force and a regularly modulated electron beam is located in the central region. The density of this electron beam is about the initial plasma density with $n_e = 1.8n_c$. Along the channel walls, it is noted that surface waves are excited. The electrons can be preaccelerated and then injected into the plasma channel by these surface waves [51,52]. In the plasma channel, the injected electrons resonantly interact with the laser pulse and gain energy continuously until dephasing

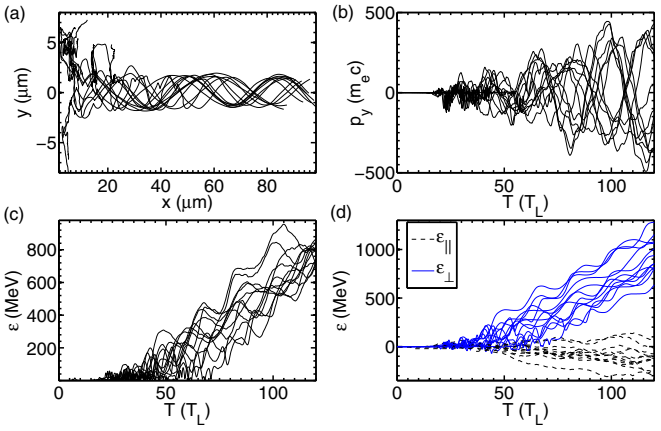

FIG. 2. (a) The trajectories of the electrons with a high energy above 700 MeV at $T = 120T_L$. (b) The corresponding evolutions of the transverse momentum of the tracing electrons. (c) The corresponding evolutions of the energy of the tracing electrons. (d) The energy gain of the tracing electrons in longitudinal direction $\epsilon_\parallel = -\int_0^t ev_x E_x dt$ and perpendicular direction $\epsilon_\perp = -\int_0^t e(v_y E_y + v_z E_z)dt$.

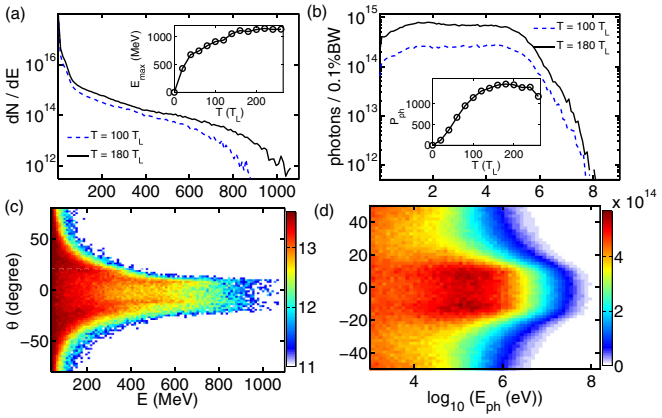

FIG. 3. (a) The energy spectrum of the electrons at two different times. (b) The corresponding spectrum of photon number calculated in 0.1% bandwidth (BW). The inset in (a) shows the evolution of the maximum energy of the electrons and the inset in (b) shows the evolution of the total radiation power $P_{\rm ph} = W_{\rm ph}/T_L$, which is defined as the emitted photon energy per laser period. (c) and (d) show the angular-spectral distribution of the electrons and the emitted photons, respectively. Here θ is defined as $\theta = \arctan(p_y/p_x)$.

occurs. Figure 1(d) indicates that the high-energy electrons are only those located in the plasma channel and they are microbunched with the laser wavelength. The transverse radius of the accelerated electron beam is about 2.2 μm, which is consistent with the laser beam size. For the DLA electrons their maximum transverse oscillation amplitude is limited by the laser beam radius. The magnetic field generated by the fast electrons in the plasma channel is shown in Fig. 1(b). The transverse profile shows that the static magnetic field varies linearly with the channel radius, suggesting that the assumptions in Secs. II and III are reasonable. The slope of the magnetic field is $\kappa_B \approx e\mu_0 n_e c/2 \approx m_e\omega_p^2/2ce$, corresponding to $f \approx 1$. This gives a maximum value of the magnetic field as $B_{Sz\max} \approx e\mu_0 n_e cR/2 \approx 3.5\times10^4 \times \frac{n_e}{n_c} R[\mu\text{m}] \approx 1.38\times10^5$ T. This corresponds to a normalized value about 13.2, which agrees well with the simulation result shown in Fig. 1(b). The fast electrons are confined by this strong magnetic field and experience transverse oscillations in the plasma channel.

Particle tracking was also performed to have an insight into the acceleration process of the high-energy electrons. Figure 2(a) shows the typical trajectories of high-energy electrons, which are mainly injected from the front surface of the plasma [31]. They experience betatron oscillations in the plasma channel. These electrons directly interact with the laser pulse in the plasma channel and both the transverse momentum and energy experience a growing process, as shown in Figs. 2(b) and 2(c). To clarify the source of energy gain of these high-energy electrons, the energy gain of each electron is separated into two parts, i.e., $\epsilon = \epsilon_\parallel + \epsilon_\perp$, where $\epsilon_\parallel = -\int_0^t e v_x E_x dt$ and $\epsilon_\perp = -\int_0^t e(v_y E_y + v_z E_z)dt$. Figure 2(d) clearly demonstrates that DLA is the main acceleration mechanism for these high-energy electrons. That is, the electrons in the plasma channel are mainly accelerated by the transverse laser electric field. Figures 3(a) and 3(b) show the energy spectra of electrons and radiated photons. The Maxwellian spectrum shown in Fig. 3(a) is also a characteristic of the direct-laser-accelerated electrons [25–30]. The inset in Fig. 3(a) shows the time evolution of the maximum electron energy. The electron energy increases dramatically at the beginning, then gradually becomes saturated at about $T = 180T_L$. The corresponding maximum energy of the electron is about $E_{\max} = \gamma_{\max} m_e c^2 \approx 1.08\frac{a_0^2}{n} m_e c^2 = 1.1$ GeV, which corresponds to a resonance condition as $\omega_\beta/\omega_L \approx 0.96$. This indicates that the betatron frequency of the electron is very close to the Doppler-shifted laser frequency, ensuring that the electron can resonantly interact with the laser field in the plasma channel. As the electrons are accelerated, both the energy and the number of emitted photons are increased, as shown in Fig. 3(b). Here all the emitted photons in the simulation box are calculated and described in order to investigate the scaling of radiation properties. The photon spectra display as synchrotronlike spectra. The inset in Fig. 3(b) shows that the radiation power becomes saturated when the electron acceleration process is terminated. In this case, the photon spectrum can be extended into the region of γ rays. The maximum photon energy approaches about 100 MeV. Figures 3(c) and 3(d) show the angular-spectral distribution of the electrons and emitted photons. These indicate that both the high-energy electrons and photons are collimated within an emission angle below 20° ($\pi/9$).

To study the parameter dependence of betatron radiation, different laser intensities and plasma densities were input into the simulations. The simulation results are shown in Figs. 4–9. Figure 4 shows the density distributions of the electrons for a fixed parameter $n/a_0 = 0.03$ but with different laser amplitudes. Figures 4(a), 4(c), and 4(e) show that the normalized density distribution and the channel length are almost the same for three different cases. Figures 4(b), 4(d), and 4(f) show that the accelerated electron beam exhibits collective motion in the plasma channel, which is microbunched with the laser

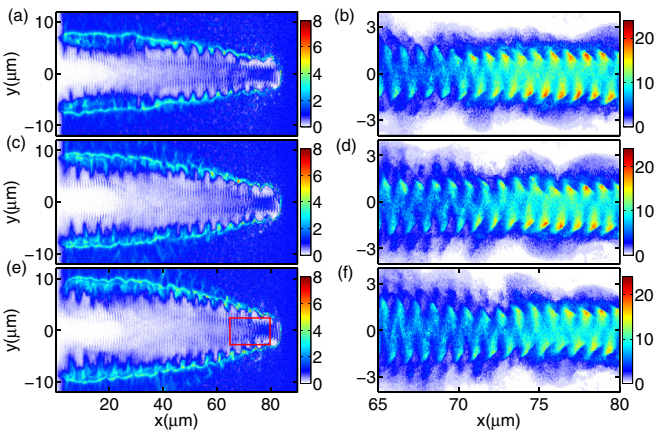

FIG. 4. The electron dynamics at $T = 100T_L$ for a fixed value of $n/a_0 = 0.03$ but with different laser intensities. (a), (c), and (e) The normalized density (n_e/n_0) distribution of the electrons. (b), (d), and (f) The corresponding normalized energy ($E_e/a_0 m_e c^2$) distribution of the electrons in the red rectangle region shown in (e). (a) and (b) The simulation result for $a_0 = 20$ and $n_e = 0.6n_c$. (c) and (d) The simulation result for $a_0 = 40$ and $n_e = 1.2n_c$. (e) and (f) The simulation result for $a_0 = 60$ and $n_e = 1.8n_c$.

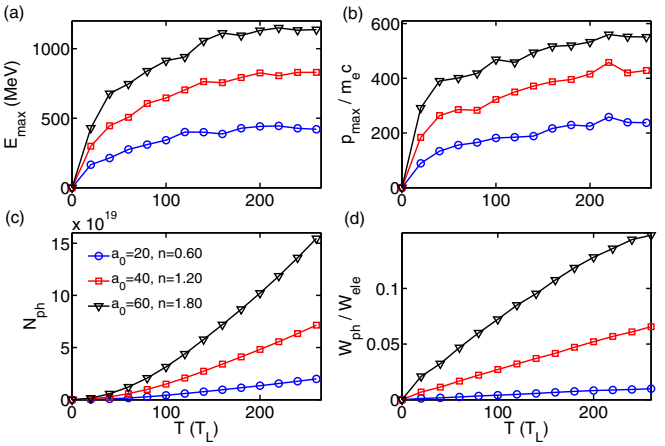

FIG. 5. The evolutions of the maximum electron energy (a), the maximum electron transverse momentum (b), the total number of radiated photons (c), and the energy conversion efficiency of the photons from the electrons (d) for a fixed value of $n/a_0 = 0.03$.

wavelength. The normalized energy distribution and transverse beam sizes are also the same in these three cases. This indicates that the electron dynamics are self-similar for a fixed value of n/a_0, which agrees well with our theoretical predictions. Once the parameter n/a_0 is fixed, the phase velocity of the laser pulse, the electron beam radius, and the betatron frequency of the resonant electron are all determined. The time evolutions of the electron dynamics and radiated photons for a fixed parameter $n/a_0 = 0.03$ also display similar behavior, as shown in Fig. 5. Figure 5(a) shows that the electron acceleration processes for different laser intensities become saturated at the same time because the acceleration time is only dependent on the value of n/a_0, as predicted by the theory. In addition, Fig. 5(b) indicates that an extremely large betatron strength parameter can be achieved in the DLA regime. It is noted from Figs. 5(a) and 5(b) that both the electron transverse momentum and energy are proportional to the laser amplitude. As a result, the betatron radiation displays a nonlinear correlation on the laser amplitude, as demonstrated in Figs. 5(c) and 5(d). Figure 6 shows the corresponding energy spectra of electrons and radiated photons. It is shown from Fig. 6(a) that the electron temperature is increased with the increase of the laser amplitude. This is strongly indicative of DLA. Figure 6(b) shows that the photon energy spectra are very sensitive to the laser intensity and can be tunable by increasing the laser amplitude.

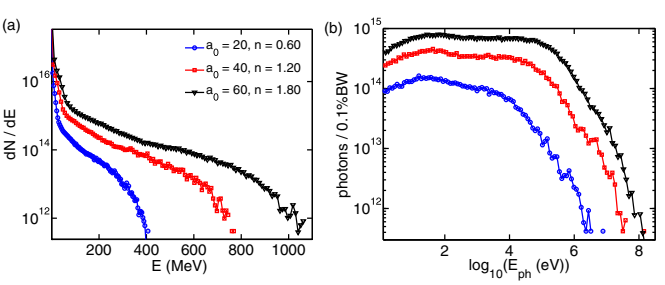

FIG. 6. The energy spectra of the electrons (a) and radiated photons (b) at $T = 180T_L$ for a fixed value of $n/a_0 = 0.03$.

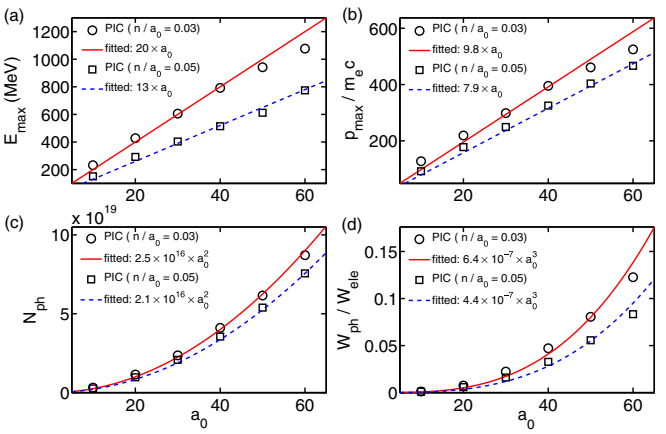

FIG. 7. The scaling properties of the electron dynamics and radiated photons for a fixed value of $n/a_0 = 0.03$ and $n/a_0 = 0.05$.

The scaling properties of the electron dynamics and radiated photons are shown in Fig. 7. For a fixed value of n/a_0, both the electron energy and transverse momentum are proportional to the laser amplitude. From Fig. 7(a) one can give an estimation of the maximum electron energy that can be accelerated in the plasma channel as $E_{\max} \approx 1.17\frac{a_0^2}{n}m_e c^2$. For a fixed value of $n/a_0 = 0.03$, this indicates that GeV electron beams can be easily achieved by using a laser pulse with an intensity above 3×10^{21} W/cm^2. Figure 7(b) shows that the betatron strength can be enhanced dramatically in the DLA regime, which is crucial to produce a radiation source with high photon energies and high photon flux. As the betatron radiation is strongly dependent on both the electron energy and transverse momentum, the total number and energy of the radiated photons display nonlinear scalings on the laser amplitude, as shown in Figs. 7(c) and 7(d). Particularly, the total number of photons scales as $N_{\rm ph} \propto a_0^2$ and the energy conversion efficiency of photons scale as $W_{\rm ph}/W_{\rm ele} \propto a_0^3$ when the parameter n/a_0 is fixed. This is in good agreement with the theoretical scalings and these nonlinear scalings are quite different from that in the laser-wakefield acceleration regime [3]. The fitted scaling shown in Fig. 7(d) suggests that 10% of the electron energy can be converted into the high-energy photons when the laser intensity is above 5×10^{21} W/cm^2. Figure 7 also indicates that the efficiencies of the electron acceleration process and the emitted radiation would be decreased for a larger value of n/a_0. For the parameters considered here, the simulation results can agree well with the theoretical scalings. However, with the increase of the laser intensity, the radiation recoil effect [53] would gradually affect the betatron radiation properties. Our further simulation results demonstrate that for a fixed value of $S = 0.03$, when the laser amplitude (a_0) is lager than 100, i.e., $a_0 > 100$, the simulation results would deviate from the theoretical scalings. This indicates that the radiation recoil effect begins to affect the electron dynamics. In the radiation reaction dominant regime, the scalings of radiation properties would become different from that in Eqs. (5) and (6). This will be discussed in detail in a future work.

Figures 8 and 9 show simulation results for a fixed laser amplitude $a_0 = 60$ but with different plasma densities. Figure 8(a) shows that the maximum electron energy that can

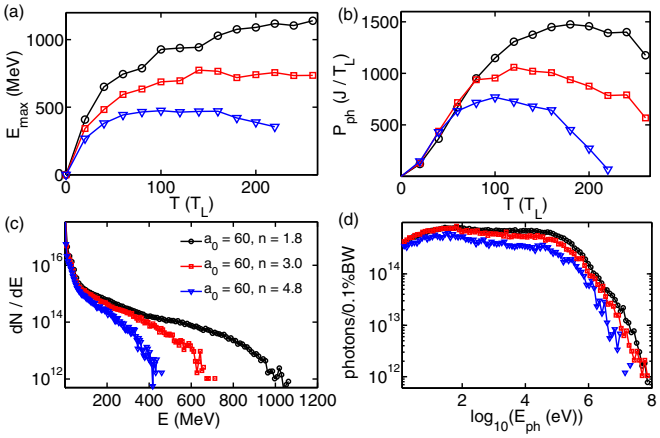

FIG. 8. The time evolutions of the maximum electron energy (a) and the total radiation power of the photons (b) for a fixed laser amplitude of $a_0 = 60$. (c) and (d) show the corresponding energy spectra of the electrons and radiated photons at the acceleration time.

be accelerated is decreased with the increase of the plasma density. The acceleration length, which is dependent on the value of n/a_0, is also decreased when the plasma density is increased. The radiation power also falls when the electron acceleration process is terminated, as shown in Fig. 8(b). The radiation power reaches the maximum value when the electron achieves its maximum energy. Figures 8(c) and 8(d) show that when the plasma density is increased, the electron temperature is decreased, as well as the number and energy of the radiated photons. But it is noted that the photon energy spectra do not change significantly, which indicates that the radiated photons are not as sensitively dependent on the plasma density as on the laser amplitude. Figure 9 shows the corresponding scaling properties of the electron dynamics and radiated photons. It is shown that for a fixed laser intensity, both the electron and radiation properties are inversely proportional to the plasma density. The maximum electron energy scales as $E_{\max} \propto \frac{a_0}{n}$, the maximum electron transverse momentum scales as $p_{\max} \propto (\frac{a_0}{n})^{0.5}$, the total number of photons scale as $N_{\rm ph} \propto (\frac{a_0}{n})^{0.5}$, and the energy conversion efficiency of photons scale as $W_{\rm ph}/W_{\rm ele} \propto \frac{a_0}{n}$. These scalings agree well with the theoretical predictions. It is noted from Fig. 9 that the presented simulations have verified the scaling properties in the range of $0.02 \leqslant S \leqslant 0.08$. Our further simulation results show that the scalings in Eqs. (5) and (6) are still applicable for $0.005 \leqslant S \leqslant 0.1$, which corresponds to the near-critical density plasma. In principle, the scalings are valid for a wide range of S. However, for a very small value of S, which corresponds to the underdense plasma, the laser wakefield acceleration becomes the dominant process. On the other hand, when the value of S is very large, the plasma becomes opaque; in this case, the electron acceleration would become inefficient. Thus, in the experiments, in order to efficiently exploit the DLA regime, the value of S should be in a suitable region ($0.005 \leqslant S \leqslant 0.1$).

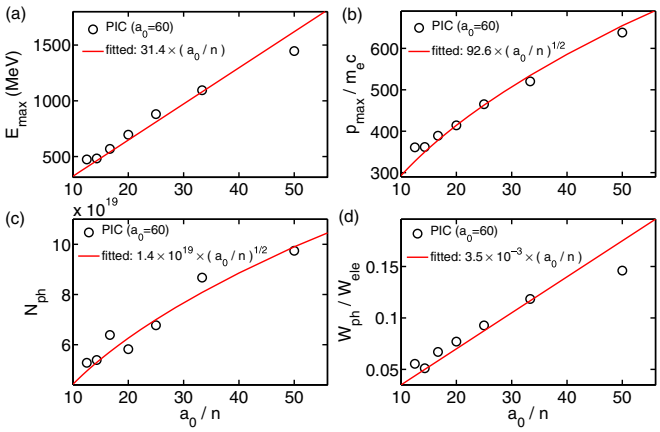

FIG. 9. The scaling properties of the electron dynamics and radiated photons at different acceleration times for a fixed laser amplitude of $a_0 = 60$.

Based on the scaling properties, one can conclude that by exploiting the DLA regime, it would be much easier to obtain an electron beam with high energy and high density, and also a radiation source with high photon energies and high photon flux by increasing the laser amplitude or decreasing the plasma density. To demonstrate the feasibility of producing a high-energy and high-flux radiation source in the DLA regime, three-dimensional particle-in-cell simulations were also performed. The simulation box has dimensions $160 \times 20 \times 20$ μm with a grid of $1920 \times 200 \times 200$ cells and eight particles of each species per cell. The laser and plasma parameters are the same as those in Fig. 1. The simulation result is shown in Fig. 10. Figure 10(a) indicates that the high-energy electrons are microbunched with the laser wavelength. These electrons can directly gain the energy from the laser field. The corresponding energy spectrum of emitted photons is shown in Fig. 10(b). The photon energy can reach about 100 MeV, which is similar to the spectrum in the 2D case, as shown in Fig. 3(b). In this case, the total emitted photon energy is about 1.12 J and the total energy of photons above 1 MeV is about 0.69 J. It is indicated that about 1% of the laser energy (125 J) is converted into the radiation and 0.6% of the laser energy is converted into the γ photons. The total number of high-energy photons above 1 MeV can reach about 1.23×10^{12}. In addition, the angular distribution of emitted photons shown in Fig. 10(c) demonstrates that the high-energy photons ($\geqslant 1$ MeV) are collimated within an emission angle between $\pi/18$ and $\pi/9$.

V. DISCUSSION

It is possible to enormously amplify the energy and transverse momentum of the electron in the DLA regime for a relatively small value of n/a_0 with a large laser amplitude. Exploiting this regime can produce a tunable radiation source with high photon energy and high photon flux simply by adjusting the laser amplitude. However, experimental results demonstrate that the divergence angle and transverse size of the radiation source generated in this regime are very large, and as a result, the observed brightness of such a radiation source is much less than that in the laser wakefield acceleration regime [14,15]. In order to increase the brightness and the photon energy of the radiation in the DLA regime, the laser plasma parameters, such as the laser intensity, pulse duration,

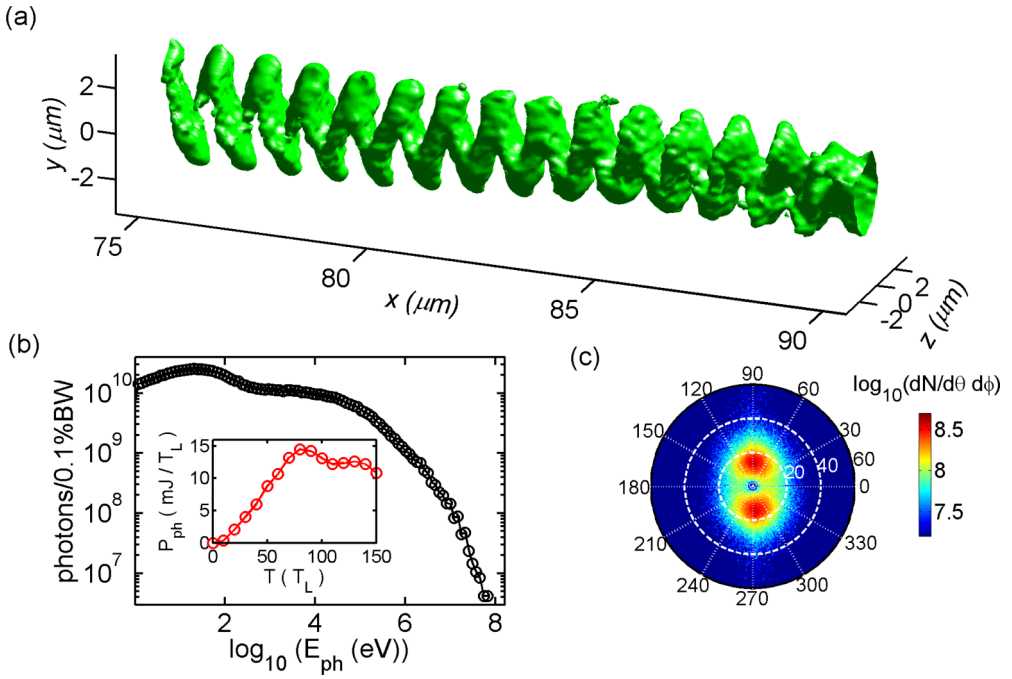

FIG. 10. 3D particle-in-cell simulation results for $a_0 = 60$ and $n_e = 1.8n_c$ at $T = 120T_L$. (a) The isosurface of the electron energy density, where the isovalue is set as $300n_cm_ec^2$. (b) The spectrum of photon number calculated in 0.1% bandwidth (BW), where the inset shows the evolution of the total radiation power $P_{\rm ph} = W_{\rm ph}/T_L$, which is defined as the emitted photon energy per laser period. (c) The angular distribution of the emitted high-energy photons ($\geqslant$1 MeV), where $\theta = \arctan(p_\perp/p_x)$, $\phi = \arctan(p_y/p_z)$, and $p_\perp = \sqrt{p_y^2 + p_z^2}$.

plasma density, and plasma length, can be further optimized. Here it is shown that the radiation source size is dependent on the transverse size of the accelerated electron beam, which depends on the acceleration length of the electrons. In the experiment, the optimization of the radiation source requires the control of the interaction length between the laser pulse and plasma.

The effective acceleration length of the DLA electron in the plasma channel is determined by the dephasing length between the electron and the laser field, and also the depletion length of the laser pulse. For the laser pulse propagating in underdense plasma, the laser energy will be depleted after a distance (depletion length) $L_{\rm etch} \approx \frac{a_0}{4n} c\tau$ [36,46], where τ is the duration of the laser pulse. The depletion length depends strongly on the choice of the pulse duration and is inversely proportional to the plasma density. On the other hand, the dephasing length between the electron and the laser field can be written as $L_{\rm dp} \approx cT_{\rm dp} \approx \frac{cT_L}{\sqrt{2}|\delta|}\frac{a_0}{n}$. The desired acceleration length for the DLA electron is the dephasing length as the electron can reach its maximum energy. This requires the laser pulse having the duration $\tau \gg \frac{4T_L}{\sqrt{2}\delta}$; here the frequency deviation is estimated to be $\delta = |1 - \frac{\omega_\beta}{\omega_L}| \approx |1 - \frac{a_0}{\sqrt{\gamma n}}|$. For the parameters in Fig. 11, this gives a value of about $\delta \approx 0.16$. In this case, $L_{\rm etch}(\approx 417\ \mu{\rm m}) \gg L_{\rm dp}$, the acceleration length for the electron is determined by the dephasing length with $L_{\rm dp} \approx 74\ \mu$m, which agrees well with the simulation result shown in Fig. 11. After this distance, the high-energy electrons overtake the laser pulse and leave the plasma channel. Those electrons with a large transverse momentum then cannot be confined in the background plasma without the channel field and they would spread away quickly in the background plasma, as shown in Fig. 11(c). As a result, the transverse size of the electron beam is expanded and the energy is also dissipated when the interaction length is larger than the dephasing length [54]. In this case, the radiation power would be reduced.

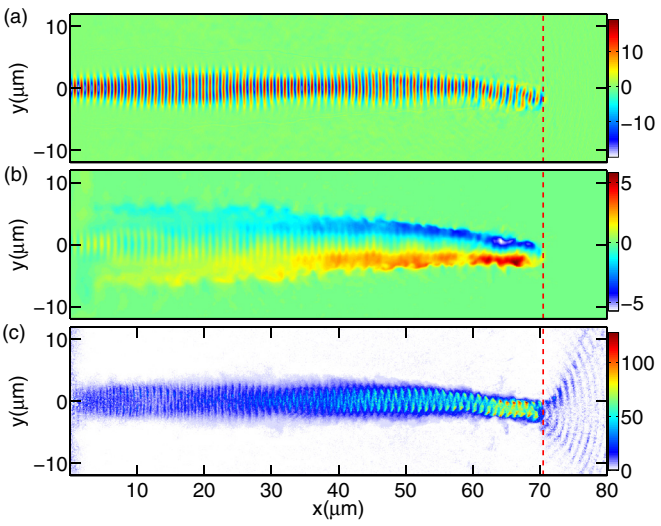

FIG. 11. The simulation result for $a_0 = 20$ and $n_e = 1.2n_c$ at $T = 100T_L$. The duration of the laser pulse is set as $100T_L$. (a) The distribution of the normalized transverse laser field ($eE_y/m_e\omega_0 c$). (b) The corresponding transverse static magnetic field ($eB_{Sz}/m_e\omega_0$). (c) The distribution of the averaged electron energy (E_e) on the grids, where the unit is MeV. The white dashed lines indicate the position of the wave front of the laser pulse.

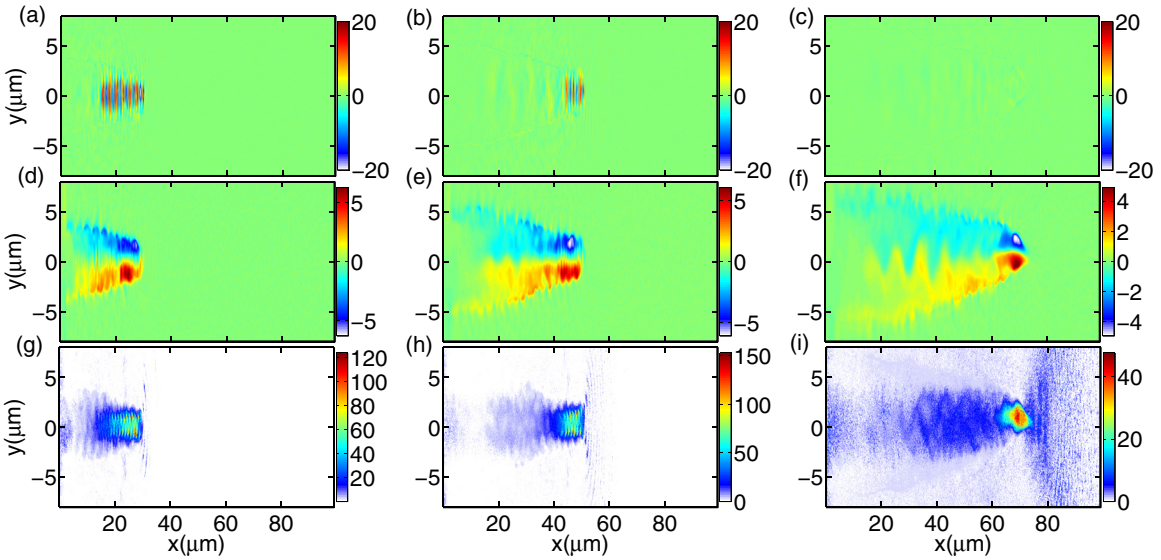

FIG. 12. The simulation result for $a_0 = 20$ and $n_e = 1.2n_c$ at $T = 40T_L$ [(a), (d), and (g)], $T = 70T_L$ [(b), (e), and (h)], and $T = 110T_L$ [(c), (f), and (i)], respectively. The duration of the laser pulse is set as $25T_L$. (a)–(c) The distribution of the normalized transverse laser field ($eE_y/m_e\omega_0 c$) at three different times. (d)–(f) The corresponding transverse static magnetic field ($eB_{Sz}/m_e\omega_0$). (g)–(i) The distribution of the averaged electron energy (E_e) on the grids.

When the depletion length for a short laser pulse is comparable to the dephasing length, pulse depletion has an important influence on the electron dynamics. Figure 12 shows the simulation result with the same parameters as in Fig. 11 but with a short pulse duration of $\tau = 25T_L$. It is noted that as the laser pulse is gradually depleted in the plasma, the longitudinal length of the high-energy electron beam is also reduced. Figure 12(c) shows that the laser pulse is completely depleted at $T = 110T_L$. At this moment, the electron acceleration process is terminated and the electron beam is not microbunched, as shown in Fig. 12(i). In addition, channel propagation ceases and the strength of the channel field is also reduced, as shown in Fig. 12(f). In this case, the relativistic electron beam would deviate from the plasma channel and these electrons with large transverse momenta cannot be confined in the plasma. Figures 12(g)–12(i) indicate that the energy of the electron beam is quickly dissipated in the plasma and the transverse beam size is also increased. This broad electron beam would result in a radiation source with a large transverse size and divergence angle. The corresponding brightness would also be reduced.

Thus, there should be an optimized interaction length in the experiment. A matching condition between the laser and plasma target parameters should be chosen so that the laser-plasma interaction and the effective electron acceleration of DLA terminate at the same time. In this case, the electron beam can be accelerated adequately and the radiation can be efficiently emitted. This optimized interaction length is determined by the dephasing length between the electron and the laser field, and also the laser depletion length in plasmas. In the practical experiment, since most of the laser and plasma target parameters are now controllable [52,55,56], the optimization is realistic. This kind of optimization would induce a radiation source with higher photon energy and higher brightness.

VI. SUMMARY

In summary, we have investigated the scaling properties of the direct-laser-accelerated electrons and the radiated photons in the DLA regime. The dependence of the radiation properties on some controllable parameters, such as the plasma density and laser intensity, as well as the interaction length, has been studied both analytically and numerically. Results have been presented confirming that the electron dynamics and the betatron radiation are strongly dependent on a self-similar parameter $S \equiv \frac{n_e}{n_c a_0}$. This controls the energy gain and the transverse betatron amplitude of the electrons, as well as the radiated photon number and photon energy. In addition, the total number and energy of the photons display nonlinear scalings on the laser amplitude for a fixed value of S. It is suggested that by exploiting the DLA regime, a tunable radiation source with high photon energy and high photon flux can be achieved by employing a relatively small value of S with a large laser amplitude. The interaction length between the laser pulse and the plasma is also suggested to be an important parameter to affect the properties of the electron beams and the radiation source. The optimization of the radiation source also requires the control of this parameter.

ACKNOWLEDGMENTS

This work was supported by the National Natural Science Foundation of China (Grants No. 91230205, No. 11575031, No. 11575298, and No. 11175026), the National Basic Research Program of China (973 Program: Grants No. 2013CBA01500 and No. 2013CB834100), and the National High-Tech 863 Project. B.Q. acknowledges the support from Thousand Young Talents Program of China. The authors acknowledge support from STFC Central Laser Facility and the Scientific Computing Department, as well as the use of

the SCARF computing cluster at STFC Rutherford-Appleton Laboratory and the support from China Scholarship Council. We would like to thank Robbie Scott, Holger Schmitz, and Raoul Trines for useful discussions. T.W.H. would also like to thank Naren Ratan, Luke Ceurvorst, Muhammad Kasim, James Sadler, Jimmy Holloway, and Matthew Levy at Oxford University and C. Z. Xiao, K. D. Xiao, K. Q. Pan, H. X. Chang, F. L. Zheng, Y. X. Zhang, W. P. Yao, and Z. Xu at Peking University for their help and guidance in this work.

[1] N. Bloembergen, Rev. Mod. Phys. **71**, S283 (1999).
[2] A. Rousse, C. Rischel, and J.-C. Gauthier, Rev. Mod. Phys. **73**, 17 (2001).
[3] S. Corde, K. Ta Phuoc, G. Lambert, R. Fitour, V. Malka, A. Rousse, A. Beck, and E. Lefebvre, Rev. Mod. Phys. **85**, 1 (2013).
[4] K. Ta Phuoc, F. Burgy, J.-P. Rousseau, V. Malka, A. Rousse, R. Shah, D. Umstadter, A. Pukhov, and S. Kiselev, Phys. Plasmas **12**, 023101 (2005).
[5] E. Esarey, B. A. Shadwick, P. Catravas, and W. P. Leemans, Phys. Rev. E **65**, 056505 (2002).
[6] I. Kostyukov, S. Kiselev, and A. Pukhov, Phys. Plasmas **10**, 4818 (2003).
[7] S. Kiselev, A. Pukhov, and I. Kostyukov, Phys. Rev. Lett. **93**, 135004 (2004).
[8] A. Rousse, K. T. Phuoc, R. Shah, A. Pukhov, E. Lefebvre, V. Malka, S. Kiselev, F. Burgy, J. P. Rousseau, D. Umstadter, and D. Hulin, Phys. Rev. Lett. **93**, 135005 (2004).
[9] H.-P. Schlenvoigt, K. Haupt, A. Debus, F. Budde, O. Jäckel, S. Pfotenhauer, H. Schwoerer, E. Rohwer, J. G. Gallacher, E. Brunetti, R. P. Shanks, S. M. Wiggins, and D. A. Jaroszynski, Nat. Phys. **4**, 130 (2008).
[10] S. Fourmaux, S. Corde, K. Ta Phuoc, P. M. Leguay, S. Payeur, P. Lassonde, S. Gnedyuk, G. Lebrun, C. Fourment, V. Malka, S. Sebban, A. Rousse, and J. C. Kieffer, New J. Phys. **13**, 033017 (2011).
[11] A. G. Khachatryan, F. A. van Goor, and K.-J. Boller, New J. Phys. **10**, 083043 (2008).
[12] F. Albert, B. B. Pollock, J. L. Shaw, K. A. Marsh, J. E. Ralph, Y. H. Chen, D. Alessi, A. Pak, C. E. Clayton, S. H. Glenzer, and C. Joshi, Phys. Rev. Lett. **111**, 235004 (2013).
[13] J. P. Palastro, D. Kaganovich, and D. Gordon, Phys. Plasmas **22**, 063111 (2015).
[14] S. Kneip, C. McGuffey, J. L. Martins, S. F. Martins, C. Bellei, V. Chvykov, F. Dollar, R. Fonseca, C. Huntington, G. Kalintchenko, A. Maksimchuk, S. P. D. Mangles, T. Matsuoka, S. R. Nagel, C. A. J. Palmer, J. Schreiber, K. Ta Phuoc, A. G. R. Thomas, V. Yanovsky, L. O. Silva, K. Krushelnick, and Z. Najmudin, Nat. Phys. **6**, 980 (2010).
[15] S. Kneip, S. R. Nagel, C. Bellei, N. Bourgeois, A. E. Dangor, A. Gopal, R. Heathcote, S. P. D. Mangles, J. R. Marques, A. Maksimchuk, P. M. Nilson, K. T. Phuoc, S. Reed, M. Tzoufras, F. S. Tsung, L. Willingale, W. B. Mori, A. Rousse, K. Krushelnick, and Z. Najmudin, Phys. Rev. Lett. **100**, 105006 (2008); S. Kneip *et al.*, Proc. SPIE **7359**, 73590T (2009).
[16] L. M. Chen, W. C. Yan, D. Z. Li, Z. D. Hu, L. Zhang, W. M. Wang, N. Hafz, J. Y. Mao, K. Huang, Y. Ma, J. R. Zhao, J. L. Ma, Y. T. Li, X. Lu, Z. M. Sheng, Z. Y. Wei, J. Gao, and J. Zhang, Sci. Rep. **3**, 1912 (2013).
[17] H. Y. Wang, B. Liu, X. Q. Yan, and M. Zepf, Phys. Plasmas **22**, 033102 (2015); B. Liu, R. H. Hu, H. Y. Wang, D. Wu, J. Liu, J. E. Chen, J. Meyer-ter-Vehn, X. Q. Yan, and X. T. He, *ibid.* **22**, 080704 (2015).
[18] A. G. R. Thomas and K. Krushelnick, Phys. Plasmas **16**, 103103 (2009).
[19] I. Nam, M. S. Hur, H. S. Uhm, N. A. M. Hafz, and H. Suk, Phys. Plasmas **18**, 043107 (2011).
[20] X. Zhang, V. N. Khudik, and G. Shvets, Phys. Rev. Lett. **114**, 184801 (2015).
[21] S. P. D. Mangles, A. G. R. Thomas, M. C. Kaluza, O. Lundh, F. Lindau, A. Persson, F. S. Tsung, Z. Najmudin, W. B. Mori, C. G. Wahlstrom, and K. Krushelnick, Phys. Rev. Lett. **96**, 215001 (2006).
[22] K. TaPhuoc, S. Corde, R. Shah, F. Albert, R. Fitour, J. P. Rousseau, F. Burgy, B. Mercier, and A. Rousse, Phys. Rev. Lett. **97**, 225002 (2006).
[23] K. Nemeth, B. Shen, Y. Li, H. Shang, R. Crowell, K. C. Harkay, and J. R. Cary, Phys. Rev. Lett. **100**, 095002 (2008).
[24] S. Cipiccia, M. R. Islam, B. Ersfeld, R. P. Shanks, E. Brunetti, G. Vieux, X. Yang, R. C. Issac, S. M. Wiggins, G. H. Welsh, M.-P. Anania, D. Maneuski, R. Montgomery, G. Smith, M. Hoek, D. J. Hamilton, N. R. C. Lemos, D. Symes, P. P. Rajeev, V. O. Shea, J. M. Dias, and D. A. Jaroszynski, Nat. Phys. **7**, 867 (2011).
[25] C. Gahn, G. D. Tsakiris, A. Pukhov, J. Meyer-ter-Vehn, G. Pretzler, P. Thirolf, D. Habs, and K. J. Witte, Phys. Rev. Lett. **83**, 4772 (1999).
[26] G. D. Tsakiris, C. Gahn, and V. K. Tripathi, Phys. Plasmas **7**, 3017 (2000).
[27] S. P. D. Mangles, B. R. Walton, M. Tzoufras, Z. Najmudin, R. J. Clarke, A. E. Dangor, R. G. Evans, S. Fritzler, A. Gopal, C. Hernandez-Gomez, W. B. Mori, W. Rozmus, M. Tatarakis, A. G. R. Thomas, F. S. Tsung, M. S. Wei, and K. Krushelnick, Phys. Rev. Lett. **94**, 245001 (2005).
[28] A. Pukhov, Z. M. Sheng, and J. Meyer-ter-Vehn, Phys. Plasmas **6**, 2847 (1999).
[29] B. Qiao, X. T. He, S.-P. Zhu, and C. Y. Zheng, Phys. Plasmas **12**, 083102 (2005); H. Y. Niu, X. T. He, B. Qiao, and C. T. Zhou, Laser Part. Beams **26**, 51 (2008).
[30] B. Liu, H. Y. Wang, J. Liu, L. B. Fu, Y. J. Xu, X. Q. Yan, and X. T. He, Phys. Rev. Lett. **110**, 045002 (2013).
[31] R. H. Hu, B. Liu, H. Y. Lu, M. L. Zhou, C. Lin, Z. M. Sheng, C.-E. Chen, X. T. He, and X. Q. Yan, Sci. Rep. **5**, 15499 (2015).
[32] S. P. D. Mangles, C. D. Murphy, Z. Najmudin, A. G. R. Thomas, J. L. Collier, A. E. Dangor, E. J. Divall, P. S. Foster, J. G. Gallacher, C. J. Hooker, D. A. Jaroszynski, A. J. Langley, W. B. Mori, P. A. Norreys, F. S. Tsung, R. Viskup, B. R. Walton, and K. Krushelnick, Nature (London) **431**, 535 (2004).
[33] C. G. R. Geddes, Cs. Toth, J. van Tilborg, E. Esarey, C. B. Schroeder, D. Bruhwiler, C. Nieter, J. Cary, and W. P. Leemans, Nature (London) **431**, 538 (2004).
[34] J. Faure, Y. Glinec, A. Pukhov, S. Kiselev, S. Gordienko, E. Lefebvre, J.-P. Rousseau, F. Burgy, and V. Malka, Nature (London) **431**, 541 (2004).
[35] E. Esarey, C. B. Schroeder, and W. P. Leemans, Rev. Mod. Phys. **81**, 1229 (2009).

[36] W. Lu, M. Tzoufras, C. Joshi, F. S. Tsung, W. B. Mori, J. Vieira, R. A. Fonseca, and L. O. Silva, Phys. Rev. ST Accel. Beams **10**, 061301 (2007).
[37] A. Pukhov and J. Meyer-ter-Vehn, Appl. Phys. B **74**, 355 (2002).
[38] C. A. Coverdale, C. B. Darrow, C. D. Decker, W. B. Mori, K. C. Tzeng, K. A. Marsh, C. E. Clayton, and C. Joshi, Phys. Rev. Lett. **74**, 4659 (1995).
[39] A. Modena, Z. Najmudin, A. E. Dangor, C. E. Clayton, K. A. Marsh, C. Joshi, V. Malka, C. B. Darrow, C. Danson, D. Neely, and F. N. Walsh, Nature (London) **377**, 606 (1995).
[40] K.-C. Tzeng, W. B. Mori, and T. Katsouleas, Phys. Rev. Lett. **79**, 5258 (1997); D. Gordon, K. C. Tzeng, C. E. Clayton, A. E. Dangor, V. Malka, K. A. Marsh, A. Modena, W. B. Mori, P. Muggli, Z. Najmudin, D. Neely, C. Danson, and C. Joshi, *ibid.* **80**, 2133 (1998).
[41] A. P. L. Robinson, A. V. Arefiev, and D. Neely, Phys. Rev. Lett. **111**, 065002 (2013).
[42] A. V. Arefiev, B. N. Breizman, M. Schollmeier, and V. N. Khudik, Phys. Rev. Lett. **108**, 145004 (2012); A. V. Arefiev, V. N. Khudik, and M. Schollmeier, Phys. Plasmas **21**, 033104 (2014).
[43] I. Kostyukov, A. Pukhov, and S. Kiselev, Phys. Plasmas **11**, 5256 (2004).
[44] W. Lu, C. Huang, M. Zhou, M. Tzoufras, F. S. Tsung, W. B. Mori, and T. Katsouleas, Phys. Plasmas **13**, 056709 (2006).
[45] T. W. Huang, A. P. L. Robinson, B. Qiao, B. Liu, A. V. Arefiev, C. T. Zhou, X. T. He, and P. A. Norreys (unpublished).
[46] A. Pukhov, Rep. Prog. Phys. **66**, 47 (2003); S. Gordienko and A. Pukhov, Phys. Plasmas **12**, 043109 (2005).
[47] T. W. Huang, C. T. Zhou, and X. T. He, Laser Part. Beams **33**, 347 (2015); T. W. Huang, C. T. Zhou, A. P. L. Robinson, B. Qiao, H. Zhang, S. Z. Wu, H. B. Zhuo, P. A. Norreys, and X. T. He, Phys. Rev. E **92**, 053106 (2015).
[48] G.-Z. Sun, E. Ott, Y. C. Lee, and P. Guzdar, Phys. Fluids **30**, 526 (1987).
[49] H. Y. Wang, C. Lin, Z. M. Sheng, B. Liu, S. Zhao, Z. Y. Guo, Y. R. Lu, X. T. He, J. E. Chen, and X. Q. Yan, Phys. Rev. Lett. **107**, 265002 (2011).
[50] T. D. Arber, K. Bennett, C. S. Brady, A. Lawrence-Douglas, M. G. Ramsay, N. J. Sircombe, P. Gillies, R. G. Evans, H. Schmitz, A. R. Bell, and C. P. Ridgers, Plasma Phys. Controlled Fusion **57**, 113001 (2015).
[51] N. Naseri, D. Pesme, W. Rozmus, and K. Popov, Phys. Rev. Lett. **108**, 105001 (2012).
[52] L. Willingale, P. M. Nilson, A. G. R. Thomas, J. Cobble, R. S. Craxton, A. Maksimchuk, P. A. Norreys, T. C. Sangster, R. H. H. Scott, C. Stoeckl, C. Zulick, and K. Krushelnick, Phys. Rev. Lett. **106**, 105002 (2011); L. Willingale, A. G. R. Thomas, P. M. Nilson, H. Chen, J. Cobble, R. S. Craxton, A. Maksimchuk, P. A. Norreys, T. C. Sangster, R. H. H. Scott, C. Stoeckl, C. Zulick, and K. Krushelnick, New J. Phys. **15**, 025023 (2013).
[53] L. L. Ji, A. Pukhov, I. Y. Kostyukov, B. F. Shen, and K. Akli, Phys. Rev. Lett. **112**, 145003 (2014).
[54] S. Zhao, C. Lin, H. Y. Wang, H. Y. Lu, X. T. He, J. E. Chen, T. E. Cowan, and X. Q. Yan, Phys. Plasmas **22**, 073106 (2015).
[55] Y. Fukuda, A. Ya. Faenov, M. Tampo, T. A. Pikuz, T. Nakamura, M. Kando, Y. Hayashi, A. Yogo, H. Sakaki, T. Kameshima, A. S. Pirozhkov, K. Ogura, M. Mori, T. Zh. Esirkepov, J. Koga, A. S. Boldarev, V. A. Gasilov, A. I. Magunov, T. Yamauchi, R. Kodama, P. R. Bolton, Y. Kato, T. Tajima, H. Daido, and S. V. Bulanov, Phys. Rev. Lett. **103**, 165002 (2009).
[56] J. H. Bin, W. J. Ma, H. Y. Wang, M. J. V. Streeter, C. Kreuzer, D. Kiefer, M. Yeung, S. Cousens, P. S. Foster, B. Dromey, X. Q. Yan, R. Ramis, J. Meyer-ter-Vehn, M. Zepf, and J. Schreiber, Phys. Rev. Lett. **115**, 064801 (2015).